IRIS AperTO

UNIVERSITÀ DEGLI STUDI DI TORINO

AperTO - Archivio Istituzionale Open Access dell'Università di Torino

Anodic Materials for Lithium-ion Batteries: TiO2-rGO Composites for High Power Applications

This is the author's manuscript

Original Citation:

Availability:

This version is available http://hdl.handle.net/2318/1625203 since 2017-05-25T10:30:18Z

Published version:

DOI:http://dx.doi.org/10.1016/j.electacta.2017.01.190

Terms of use:

Open Access

Anyone can freely access the full text of works made available as "Open Access". Works made available under a Creative Commons license can be used according to the terms and conditions of said license. Use of all other works requires consent of the right holder (author or publisher) if not exempted from copyright protection by the applicable law.

(Article begins on next page)

24 January 2025

IRIS AperTO

UNIVERSITÀ DEGLI STUDI DI TORINO

This Accepted Author Manuscript (AAM) is copyrighted and published by Elsevier. It is posted here by agreement between Elsevier and the University of Turin. Changes resulting from the publishing process - such as editing, corrections, structural formatting, and other quality control mechanisms - may not be reflected in this version of the text. The definitive version of the text was subsequently published in ELECTROCHIMICA ACTA, 230, 2017, http://dx.doi.org/10.1016/j.electacta.2017.01.190.

You may download, copy and otherwise use the AAM for non-commercial purposes provided that your license is limited by the following restrictions:

(1) You may use this AAM for non-commercial purposes only under the terms of the CC-BY-NC-ND license.

(2) The integrity of the work and identification of the author, copyright owner, and publisher must be preserved in any copy.

(3) You must attribute this AAM in the following format: Creative Commons BY-NC-ND license (http://creativecommons.org/licenses/by-nc-nd/4.0/deed.en), http://dx.doi.org/10.1016/j.electacta.2017.01.190

When citing, please refer to the published version.

Link to this full text:
http://hdl.handle.net/2318/1625203

This full text was downloaded from iris - AperTO: https://iris.unito.it/

iris - AperTO

University of Turin's Institutional Research Information System and Open Access Institutional Repository

Anodic Materials for Lithium-ion Batteries: TiO_2-rGO Composites for High Power Applications

*M. Minella[a], D. Versaci[b], S. Casino[b], F. Di Lupo[b], C. Minero[a], A. Battiato[c], N. Penazzi[b], S. Bodoardo[b]**

[a] Department of Chemistry and NIS Inter-departmental centre, University of Torino, via P. Giuria 5, Torino,10125, Italy

[b] Gruppo di Elettrochimica - Department of Applied Science and Technology, Politecnico di Torino, c.so Duca degli Abruzzi 24, 10129 Torino, Italy

[c] Department of Physics and NIS Inter-departmental Centre, University of Torino, via P. Giuria 1, Torino, 10125, Italy

* corresponding author:

Prof. Silvia Bodoardo

Gruppo di Elettrochimica - Department of Applied Science and Technology, Politecnico di Torino, c.so Duca degli Abruzzi 24, 10129 Torino, Italy

Tel.: +39 011 090 4641, Fax: +39 011 090 4699, e-mail address: silvia.bodoardo@polito.it.

KEYWORDS: Li-ion Batteries, Anode material, High Power, TiO_2, Reduced Graphene Oxide

ABSTRACT

Titanium dioxide/reduced graphene oxide (TiO_2-rGO) composites were synthesized at different loadings of carbonaceous phase, characterized and used as anode materials in Lithium-ion cells, focusing not only on the high rate capability but also on the simplicity and low cost of the electrode production. It was therefore chosen to use commercial TiO_2, GO was synthesized from graphite, adsorbed onto TiO_2 and reduced to rGO following a chemical, a photocatalytic and an in situ photocatalytic procedure. The synthesized materials were in-depth characterized with a multi-technique approach and the electrochemical performances were correlated *i*) to an effective reduction of the GO oxidized moieties and *ii*) to the maintenance of the 2D geometry of the final graphenic structure observed. TiO_2-rGO obtained with the first two procedures showed good cycle stability, high capacity and impressive rate capability particularly at 10% GO loading. The photocatalytic reduction applied in situ on preassembled electrodes showed similarly good results reaching the goal of a further simplification of the anode production.

1. INTRODUCTION

The Li-ion batteries world has undergone marked changes during the last years, and it is continuously evolving. Limited initially by the high price, as Asian manufactures started to compete in this field after the year 2000, the cells price has drastically lowered [1] as a consequence of the increased commercial diffusion (from 2 GWh in 2000 to 34 GWh in 2012). Moreover, in the last few years the application field of the Li-ion systems has been extended from electronics and portable devices to the transportation field. This kind of cell is actually replacing the NiMH technology especially in hybrid and micro-Hybrid Electric Vehicles (micro-HEVs) [2-4]. Hybrid vehicles are today the 3% of all cars, but the most recent studies predict that their number will quickly increase in the next few years [2].

As for HEV mobility, the main requirement of the accumulator is the high power density, while energy density is secondary [3]. In this context safety comes out to be of paramount importance [1].

To optimize the Li-ion system with respect to the recalled requirements, new electrode materials have to be considered, in particular regarding the anode aiming at substituting graphite, the currently most employed anode material, which cannot sustain the high currents needed to reach high power and is limited from the safety viewpoint [5]. Recently, the attention of researchers has focused on titanium oxide, in particular its crystallographic form anatase [3,4,6-10,13], due to its high chemical stability, low cost, environmental sustainability, combined to interesting electrochemical performances, including a higher charging potential that prevents lithium dendrite formation. In fact, TiO_2 is intrinsically safer than graphite (showing a reversible intercalation of Li-ions at about 1.5 V vs. Li^+/Li) while delivering comparable theoretical capacity (around 335 mAh g^{-1}). Moreover, it reveals enhanced stability and long cycle life thanks to the negligible lattice changes during reactions [11].

A major drawback of TiO_2 is its poor conductivity. Some authors proposed different methods to overcome the poor TiO_2 anode conductivity, as embedding noble metal nano-particles on TiO_2 fibers [12] or nanostructuring TiO_2 and adding a C layer [13,14]. However, all these synthesis approaches are not suitable for an industrial scale-up, very few authors evaluated the industrial feasibility of the reported processes [5].

A huge number of references is present in the literature regarding the coupling of graphene species to TiO_2, where graphene acts as an electronic conductivity enhancer [6,7,11, 15-23]. Commonly, the TiO_2 synthesis is carried out directly *in situ* on the graphene sheets[6,7,11,15,16, 21,22,23]. Ren et al. [18] and Zhen at al. [19] reported the advantage of the use of reduced graphene oxide produced by means of a hydrothermal approach, which is currently a widely diffuse technology in the chemical industrial field, but is characterized by high energy cost. Sun et al. [20] reported the use of a TiO_2-reduced graphene oxide composite obtained in alkaline hydrothermal conditions as anodic material in LIBs, but they only partially characterized the obtained material and did not investigate the specific capacity of this material at high C-rate. Recently, Xie et al. [17] , aiming at the development of a simple and cost-effective way for synthesizing TiO_2/graphene composites, presented a one-step, one-pot solvothermal method to directly obtain TiO_2/graphene. Just for sake of completeness, we report the use of TiO_2-graphene hybrids produced by mechanical ball-milling mixing of the two phases as electroactive materials in magnesium-ion batteries [24].

The present work reports the results we have obtained, up to now, on the preparation of a TiO_2-graphene composite as anodic active material for high power Li ion cells. Such material should also be easily up-scalable to industrial level, being this aspect a key issue to the realistic application of Li-ion batteries in the automotive field [3,5].

The material preparation must be therefore simple and inexpensive. With this scope in mind, commercial anatase as raw material has been used, so to start with a product disposable in high quantities in the commerce while the added GO was prepared following previous studies. The

experimental investigations regard the characterization of samples obtained by different GO reduction strategies (chemical, photocatalytic and in situ photocatalytic) aiming at the optimization of an effective and easily scalable method to obtain high conductivity anodic material.

A similar approach has never been adopted before for Li-ion battery applications. Beyond the cited work of Xie et al. [17], representing an effective improvement in the TiO_2/graphene preparation, Qiu et al. [15] reported a one-pot hydrothermal route to obtain TiO_2 on a commercial graphene. At the best of our knowledge, only two examples are reported in the literature, regarding different applications [25,26].

We also used a high current (1C) for the first galvanostatic cycles during the electrochemical performance. The results obtained give good grounds to think that the "formation" (that is the first charge, of a freshly prepared battery, corresponding to the lithiation of TiO_2 in our case) will be effective at currents higher than those use in industry practice (e.g. C/10).

Additional experimental work was carried out to optimize the quantity of graphene added to TiO_2 obtaining markedly good results, at the same level as those reported in the previously cited literature.

2. EXPERIMENTAL SECTION

2.1. Synthesis

TiO_2 Hombikat N100 (Sachtleben, Germany), a commercial anatase nanopowder specifically developed for photocatalytic applications with a Specific Surface Area (SSA) equal to 100 $m^2\ g^{-1}$, was used as starting material for the synthesis of TiO_2-rGO composites. GO to be adsorbed onto the TiO_2 nanoparticles was synthesized by chemical exfoliation of graphite (graphite natural powder, briquetting grade, Alfa Aesar) previously oxidized with $KMnO_4$ in acidic media (H_2SO_4, H_3PO_4) according to the modified Hummers and Staudemaier's method [27,28] proposed by Huang et al. [29]. The GO suspensions obtained were purified by means of dialysis. Details on

the synthesis are reported in Minella et al. [30]. The amount of carbon in the obtained suspension was evaluated by measuring the concentration of total organic carbon (TOC) in diluted GO suspensions. This value was used to tune the carbon loading of TiO_2-rGO to 5% w/w for a comparison among the different reduction strategies. In addition, for the samples obtained by chemical and photocatalytic reduction different carbon loads were investigated ranging from 0.5% to 20% w/w. The addition of the desired amount of GO to the TiO_2 suspension destabilized the colloid due to the adsorption of GO on the titania surface causing the precipitation of the TiO_2-GO phase. The TiO_2-GO composite obtained was successively reduced following two different procedures (see below) to get TiO_2-rGO composites. The acronyms used to identify the produced samples are reported in Table 1.

The chemical reduction was carried out adding drop wise and under vigorous stirring hydrazine monohydrate to the TiO_2-GO suspension. The suspension was left under stirring at room temperature for 10 hours and its color turned from brownish to dark grey.

The photocatalytic reduction of TiO_2-GO composite was carried out in three following steps *i*) adding methanol to the suspension, *ii*) transferring it in a glass Pyrex cell, *iii*) bubbling ultrapure nitrogen to completely remove the oxygen, and finally *iv*) UV irradiating the suspension with a Philips PL-S 9W/2P PLB (irradiation time: 12 hours; irradiation power: 85 W m^{-2} in the 300-400 nm range). During irradiation, TiO_2 absorbs photons with energy greater that its band gap so promoting a band to band transition with formation of valence band holes (h^+_{vb}), which are immediately scavenged by the large excess of methanol, and conduction band electrons (e^-_{cb}) which reduced the GO oxidized moieties.

At the end of the reductive step, all the suspensions were collected and purified with the same process. They were separated by centrifugation, washed with ultrapure water, dried at 373 K for 1 hour and grinded.

An additional sample, TiO_2-rGO(photEL), was obtained preparing the anode with the TiO_2-GO composite and performing the GO photocatalytic reduction in nitrogen atmosphere directly on the pre-assembled electrode.

2.2. Structural characterization

Specific surface area and pore volume distribution were determined using respectively the Brunauer, Emmet, Teller (BET) and the Barrett–Joyner–Halenda (BJH) methods after that nitrogen adsorption–desorption isotherms at 77 K of the outgassed powders were collected with an ASAP 2010 Micromeritics instrument. Samples morphology was investigated by means of a high-resolution transmission electron microscope (HR-TEM, JEOL JEM 3010), equipped with a LaB_6 source with an accelerating voltage of 300 kV. The thermal stability of the samples was evaluated by Thermogravimetric Analysis (TGA) with a TGA/SDTA-851 thermal balance (Mettler Toledo) both in anoxic atmosphere (ultrapure N_2, 60 cm^3 min^{-1}) and in air. The heating of the samples was carried out from r.t. to 800 °C with a 10 °C min^{-1} heating rate. The crystallographic composition of all the synthesized materials was evaluated with a XRD Philips X'pert Pro spectrometer (Bragg-Brentano geometry) equipped with a Cu(K α) source (λ = 1,54 Å, 45 kV, 40 mA). The spectra were recorded in the 5-90 ° 2θ interval with a *step size* of 0,0167 ° and an acquisition time per step of 80 seconds. The Raman spectra of a selection of the synthesized samples were recorded with a micro-Raman spectrometer Labram Hrvis HR800 (Jobin Yvon) equipped with an optical microscope Olympus BX41 and a solid state Nd laser (λ=532 nm, 100 mW, 2 cm^{-1} resolution with the adopted 1800 grooves mm^{-1}).

The XPS analysis was carried out not only to confirm the elemental composition of the produced samples, but also to exploit the superior energy resolution of the ESCA-XPS technique to investigate the nature of the chemical bonds of the TiO_2-GO and TiO_2-rGO samples. The XPS spectra were recorded on pelletized samples with a VSW TA10 non-monochromatic Mg Kα X-ray

source (1253.6 eV) equipped with a VSW Class 100 Concentric Hemispherical Analyzer. The deconvolution of the C1s signal recorded on TiO_2-GO and TiO_2-rGO (5%) produced with the different reduction methods were carried out by using Gaussian components. The assignation of the signals obtained from the C1s peak fitting to the related type of chemical bond was done on the basis of the data reported in literature [31,32 and reference therein].

2.3.Electrochemical testing

Electrochemical tests were carried out on disk electrodes (1 cm diameter, about 1 mg of active material mass), cut from a thin film obtained as follow. A N-methyl-2-pyrrolidone (NMP, Aldrich) based slurry of the as-prepared TiO_2-rGO (or TiO_2-GO for TiO_2-rGO(photEL) sample) was mixed with acetylene black (Shawinigan Black AB50, Chevron Corp., USA) as electronic conduction enhancer and poly-(vinylidenefluoride) as binder (PVdF, Solvay Solef-6020), in the weight ratio of 70:20:10. The mixture was then deposited over a copper foil as current collector using a standard "doctor blade" technique. After the evaporation of the solvent, the film was hot pressed (10 minutes at 70 °C and 200 bar) in order to improve the adhesion, cut into disks and outgassed, then transferred into an Ar filled dry glove-box (MBraun Labstar, H_2O and O_2 content < 1 ppm) for cell assembly The disks, loaded with 0.9 mg approximately of active material constituted the working electrodes having a surface of 0.8 cm^2 hence the electrode loading is of ≈1.1 mg/cm^2. Polypropylene three-electrode T-cells were assembled by contacting in sequence the working electrode (having the above describe composition), a 1.0 M lithium perchlorate ($LiClO_4$, Aldrich) in a 1:1 w/w% mixture of ethylene carbonate (EC, Fluka) and diethyl carbonate (DEC, Aldrich) electrolyte soaked on a Whatman® GF/A separator and a lithium foil (high purity lithium foils, Chemetall Foote corporation) counter electrode. An additional lithium foil, acting as the reference electrode, was placed at the third opening of T-cell when cyclic voltammetry tests were carried out. Galvanostatic discharge/charge cycling tests and cyclic voltammetry characterization

were performed at ambient temperature using an Arbin instrument battery testing system model BT-2000. The galvanostatic discharge/charge cycles were carried out at current regimes ranging from 1C to 40C (1C = 335 mAg^{-1}) between the cut off potentials of 1.0 and 3.0 V vs. Li^+/Li. Both charge and discharge were set at the same C-rate. In the tests, discharge refers to the lithium insertion process in the working electrode, while charge refers to the lithium de-insertion process. During the cyclic voltammetries, carried out on newly assembled cells, the electrode potential was scanned between 1.0 and 3.0 V vs Li^+/Li at 0.1 mV s^{-1}. The scan started from the cell open circuit potential (OCP) towards lower potential values. The cycles were repeated generally five times to ensure that the processes had a constant ongoing.

3. RESULTS AND DISCUSSION

3.1. Structural and morphological investigation

Fig.1 shows the X-Ray diffractogram of TiO_2 N100, TiO_2-GO and TiO_2-rGO (chemical and photocatalytic reduction at 5% carbon loading) and of the briquetting grade graphite, raw material for the synthesis of GO. First of all, no peaks due to the presence of graphite are present in all the spectra of the composites (see as an example the absence of the high intense peak at $2\theta = 26.4°$) as a consequence of a complete exfoliation of graphite during the synthesis of GO [33]. The spectra of the composites are all dominated by the reflections related to the presence of the TiO_2 in its crystal habit of anatase without any significant change in the peak position or shape due to the reduction procedure, which, as expected, does not modify the crystallographic properties of the TiO_2 nanoparticles. Note that the low intensity peaks at $2\theta = 24.57°$ and 23.0° of GO [28] are not visible in the TiO_2-GO spectrum because of the low loading and of the overlap of this signal with the main peak of the anatase phase (25.3°). Furthermore, the spectra of TiO_2-GO, TiO_2-rGO(phot) and TiO_2-rGO(chem) show a very low intensity peak at roughly $2\theta = 10$-12°. This peak is due to the presence

of a small amount of GO [12,32,34] according to a not complete reduction of the GO structure to graphene.

Please insert here Figure 1

The morphology of the produced hybrids has been evaluated by means of high resolution transmission microscopy (HR-TEM). Fig. 2 shows the HR-TEM micrographs of TiO_2-GO (sample not reduced, Fig. 2a) and of the composites obtained after chemical and photocatalytic reduction methods (5% rGO loadings, Fig. 2b and 3c respectively). From a morphological point of view, TiO_2-GO, TiO_2-rGO(chem) and TiO_2-rGO(phot) show the same structure: TiO_2 nanoparticles (average particle size ≈20 nm) are dispersed on the 2D layers of the graphenic structure (graphene nanoplatelets) in the form of clusters of the primary particles.

Please insert here Figure 2

The employed reduction methods have different effects on the mesoporosity of the prepared samples. This is shown in Fig. 3a, where the volume pore distribution of the two TiO_2-rGO composites (5% rGO loadings) and TiO_2 N100 is reported. TiO_2-rGO(chem) and TiO_2-rGO(phot) have two main families of pores, whose size are of about 25 Å and 75 Å as for TiO_2 N100. These two TiO_2-rGO composites have a surface area (see inset of Fig. 3a) greater than the starting commercial material (110 m^2g^{-1}, 120 m^2g^{-1} for TiO_2-rGO(chem) and TiO_2-rGO(phot), respectively). It is to be noted moreover that the distribution of porosity and the specific surface area have been found to be influenced by the rGO loading. The presence of rGO increases the volume of the pores with diameter ~ 25 Å, while the average volume of the second family of pores (Ø ~ 75 Å) decreases with the increment of %rGO with a sharp change in the 10-20% range. Fig. 3b reports as an example the

results for the sample TiO_2-rGO(phot), the inset shows the change in the SSA at different rGO loadings, note that both the samples with 5% (120 m^2 g^{-1}) and 10% (113 m^2 g^{-1}) show a significant higher value for the surface area than TiO_2 N100, while the SSA value, like in the distribution of the pores, fades with a further increment of the carbonaceous phase loading (84 m^2 g^{-1} for the sample with 20% of rGO). As it will be seen in the followings, this behavior is strictly related to the electrochemical performance.

Please insert here Figure 3

The thermal stability of the TiO_2-rGO samples (5% rGO loadings) was evaluated both in air and in nitrogen with thermogravimetric analysis (TGA). The tests carried out in air, unlike those in anoxic condition, allow a complete combustion of the carbon phase confirming in this way the actual carbon loading. Fig. 4a shows the thermogravimetric profiles of the samples in air, the main losses of weight happen in two different windows of temperature. In the 100-150°C temperature range we observed a 1% of loss for the TiO_2 pristine while an higher loss, roughly 4%, was registered for the samples obtained by photocatalytic and chemical reduction. This loss can be easily related to the desorption of water slightly physisorbed at the surface of the samples. The second significant loss of weight was observed in the 400-600°C range, in these conditions the combustion of the carbonaceous structure of the rGO happens [35-38] and consequently a ~5% loss of weight was observed (note that the desired loadings of carbon in the samples was exactly 5%). The sample obtained by photocatalytic reduction shows a further loss of ~2-3% at 200°C ascribable to the presence of labile oxidized functional groups [36,39] in the graphenic structure even after the photocataltytic reduction. This suggests that the photocatalytic process with respect to the chemical one is less active in the reduction of the GO structure and consequently leaves some thermo-labile groups, which are lost at roughly ~200 °C.

In nitrogen atmosphere (Fig. 4b) the TiO_2 N100 does not show significant weight loss, with the exception of the thermal desorption of the physisorbed water at ~100 °C. The other samples show an overall loss of weight equal to 7-8 % in three different temperature ranges: 100-110, 150-200 and 450-500 °C. In the first range the desorption of the adsorbed water was observed, while in the other two ranges the thermal release of labile oxidized groups can be envisaged. Note that the thermal treatment of GO in anoxic conditions is a possible route for the reduction of GO to rGO. In pure nitrogen and at temperature of 450-500 °C the loss of oxidized moieties from GO structure is well documented [38,40].

Please insert here Figure 4

The elemental composition and the type of chemical bonds in the produced samples were investigated by ESCA-XPS. The full range XPS, the binding energy (BE) and the % atomic relative concentration of the deconvoluted components of each single photoelectric core line are reported as Supplementary Data (see Fig. S1 and Table S1-S6). Particular emphasis was paid to the C1s signals and their deconvolution (Fig. S2 and Fig. S3) from which it was possible to infer about the modifications of the oxidation state of carbon before and after the different reduction procedure concluding that the higher degree of reduction was obtained by the chemical reduction.

3.3. Electrochemical behaviour

The cyclic voltammetries (second cycle) reported in Fig. 5 for the synthesized rGO samples and pure TiO_2 show a reduction peak in the branch going towards lower potentials and an oxidation one in the branch towards higher potentials, the peak positions are reported in Table 2. These results are in accord with the literature [15,28,42] and confirm the expected electrochemical process: the main redox reaction responsible for the electrochemical activity is the reduction of Ti^{4+} to Ti^{3+}

during the discharge and vice versa the oxidation of Ti^{3+} to Ti^{4+} during the charge process. Concurrently, the Li insertion-deinsertion reaction takes place as follows [41,43]:

$$TiO_2 + xLi^+ + xe^- \rightleftarrows Li_xTiO_2$$

The voltammetric profiles for the various samples appear quite similar. In all cases the electrochemical process is reversible, anyway, some differences can be devised. In Fig. 5 TiO_2-rGO(chem) shows lower values of the peaks intensity while (see Table 2) the charge passed during reduction and oxidation is not so lower than the other cases. It can be hypothesized that the insertion-deinsertion rate of Li^+ is limited in this case not by the transfer of Li^+ ions in the electrolyte, which is the same in all cases, but by the surface conditions. This observation stems from the differences in specific surface and from the pore distribution data: as a matter of fact TiO_2-rGO(chem) shows a lower pore volume and a related larger width pores (see Fig 3a).

The values of the difference between the peaks position, taken as a measure of the influence of the overpotential and of the conductivity, are quite similar but the lowest value shown by the TiO_2-rGO(phot) sample would suggest a somehow lower influence of the conductivity limitation.

Please insert here Figure 5

The performance of the samples in terms of specific capacity and rate capability during charge and discharge was evaluated upon repeated galvanostatic cycles at different C-rates from 1C to 40C. The voltage vs. specific capacity profiles related to the 2^{nd} and 100^{th} cycles recorded respectively at 1C and 10C (plots a and b of Fig. 6) are consistent with those reported in the literature [13]. All the samples show two plateaus at about 1.75 V and 2 V vs Li^+/Li typical of

anatase, involving the phase transition tetragonal anatase TiO_2 – orthorhombic anatase $Li_{0.5}TiO_2$ with lithium insertion and viceversa [19]. As a matter of fact, although the theoretical capacity of anatase TiO_2 is 330 mAh g^{-1}, the practical achievable capacity is only half of it. This is mainly because the presence of Li higher than $x = 0.5$ in Li$x$$TiO_2$ leads to strong Li–Li interaction in the lattice [35,36,44].)

As observed comparing Fig. 6a, and b, repeated cycling does not degrade the characteristic and the behavior of the TiO_2-rGO(chem) and TiO_2-rGO(phot). The capacity after 100 cycles (the first 50 carried out at 1C, 25 at 5C and the last 25 at 10C, Fig 8c) is decreased with respect to that measured at the first cycle, but still indicates an electrochemically active electrode material. TiO_2 N100, as expected taking into account its structural-morphological features [8,42], shows good cycle stability and appreciable specific capacity values at low currents only (Fig. 6a), while it shows a dramatic capacity fade at current regimes higher than 5C, Fig. 6b.

These findings are completed by those reported in Fig. 6c. The limited decay of the capacity during the first cycles indicates that the structure of the active material stands well a high current formation, an important issue from the industrial viewpoint. The figure reports high capacity values at high current regimes in the case TiO_2-rGO(chem) and TiO_2-rGO(phot) while TiO_2 N100 ceases to cycle. The rGO composites can still deliver one third of the initial capacity, at 40C. The effect of rGO on the conductivity of the samples is typical: almost negligible at lower currents, it becomes evident from 10C rate on. The capacity profile also reveals that the structure of the samples is not damaged by the high current cycling, in fact decreasing the current to 1C, after 175 cycles, the same initial 1C capacity values can be found in all samples.

Finally, Fig. 6d reports the behavior of the TiO_2-rGO(photEL) sample, where the photocatalytic reduction of GO is carried out in situ on the electrode prepared with the mixture TiO_2-GO. For sake of comparison the curve of the TiO_2-rGO(phot) sample has been added. The

delivered specific capacities appear very close for the two samples, suggesting that it is possible to reduce the GO in a preassembled electrode allowing a further simplification of the whole process.

Please insert here Figure 6

3.3.1 Variation of the GO load

Important results in terms of performance have been obtained by varying the GO load on the electrochemical properties of TiO_2-rGO(chem) (Fig. 7a) and TiO_2-rGO(phot) (Fig. 7b). Samples were prepared with different amounts of GO ranging from 0.5% to 20% w/w. In the plots the results with different GO amounts are reported along with the capacity recorded for the commercial sample without additive. A noticeable capacity increase is obtained increasing the rGO loading up to 10% w/w, while at 20% a significant decrease is shown. It is worth noting that while most of the samples show a limited capacity decay at the first cycles, on the contrary the 10% rGO sample shows an evident decay. The reason for this is not known, it appears to be a typical behavior of that particular sample only.

Please insert here Figure 7

Fig. 8 shows the average specific capacity for each C-rate tested recorded for TiO_2-rGO(chem) (Fig. 8a) and TiO_2-rGO(phot) (Fig. 8b) as a function of the C-rate itself for the samples at 5, 10 an 20% of rGO together with the average capacity measured for TiO_2-N100. The figure can be of help in finding out some explanation for the trend with a maximum in the specific capacity as a function of %rGO. In both cases the positive effect on the conductivity of the rGO addition is shown by the similar slope of the capacity variation with the C regime of rGO containing samples. In the case of

pure TiO_2 on the contrary the slope is much steeper leading to 0 capacity at 20C. The curve of the samples at 10% rGO is similar but appears just shifted along the vertical axis with respect to 5 and 20%. Such behavior suggests that the effect of %rGO is related not to a significant change in the conductivity (as is the case for the pure TiO_2) but to the change in the active mass extent involved in the electrochemical process. The results reported in Fig 4b seem to confirm this proposition particularly for the 20% sample where the average volume of the second family of pores (Ø ~ 75 Å) appears markedly limited. The degree of porosity and the pore size distribution seem to be more important parameters than the specific surface itself.

Please insert here Figure 8

The comparison of the results of the 10% rGO sample, the most performing one, with the findings from the really extended bibliography regarding the TiO_2/graphene composites is of great importance to evaluate how near we got to our aims. Of the most recent publications [6,17,21], the paper of Xie et al. [17] is particularly important as it reports in a condensed way the best results obtained by other researchers. Examination of the results puts in evidence that the discharge specific capacity of the samples, though synthesized via a simplified procedure starting from low cost industrially produced TiO_2, differs (is lower) by not more than 20% with respect to the best results obtained in the literature, not only at low (1C) but also at high rate. Moreover, few references show good results at regimes higher than 20C, whereas we reported values up to 40C.

The results appear satisfying, however we are not interested really in the maximum performance, but we aim at obtaining a material capable of fulfilling the industrial production issues. In this light, much work is still to be accomplished in order to assure a long operating

lifetime, that is a high number of cycles [7,17,21]. Another important aspect to be considered in the industrial transfer is the relation between the performance and the industrial characteristic such as the electrode loading. As it is well known, low loading value promotes high performance during cycling for a number of reasons like f. i. the lower thickness of the electrode. Li et al. [16] report specific capacities up to 30C similar to ours but with loading (4 mg/cm^2 approx.) very near to that used in industrial LIB production, more than our 1 mg/cm^2.

4. CONCLUSIONS

In the procedure here reported Graphene Oxide (GO) was adhered to the TiO_2 surface and successively reduced to rGO with the aim to obtain the desired electrical conductivity [45]. Such material proved not only to be capable of standing a high discharge current value, i. e. 40C (complete charge or discharge in a minute and a half) but supported also a high rate (1C) regime during the initial cycling showing that a rapid formation stage is possible.

Another interesting result is the modification of the photocatalytic reduction step which was carried out directly on the anodes prepared from the TiO_2-GO composite. This is a further simplification of the process moving it closer to the industrial needs.

The performance of the material obtained via an industry-oriented process has given good results in terms of discharge specific capacity, comparable to those reported in the literature. However much work is still to be accomplished, and it is actually being carried out, to assure a high number of cycles before the end of the operating life and extend the high performance also at an industry level loading of the electrode.

Acknowledgments

Regione Piemonte is kindly acknowledged for the financial support (ca(R)vour project - DD n.729 29/10/2014) “Piattaforme innovative” P.O.R. FESR 2007 – 2013. M. Minella and C. Minero

acknowledge financial support from Università di Torino - Ricerca Locale and Dr. Gloria Berlier and Prof. Ettore Vittone for the technical support during the SSA and XPS analysis, respectively.

Supplementary data: Full range ESCA-XPS spectra and particular of C1s core lines; binding energy and % atomic relative concentration of each deconvoluted component for TiO_2- GO, TiO_2-rGO(chem) and TiO_2-rGO(phot) (all with a 5% GO/rGO loading) samples. Supplementary data associated with this article can be found, in the online version, at http://.....

Table 1. Acronyms used to identify the synthesized composites.

Acronym	*Description*
TiO_2 N100	TiO_2 Hombikat N100 (anatase)
TiO_2-GO	Composite TiO_2 N100 + 5% Graphene Oxide as synthesized
TiO_2-rGO(chem)	Composite TiO_2 N100 + 5% reduced-Graphene Oxide (chemical reduction with hydrazine)
TiO_2-rGO(phot)	Composite TiO_2 N100 + 5% reduced-Graphene Oxide (photocatalytic reduction)
TiO_2-rGO(photEL)	TiO_2-GO (70%) + acetylene black (20%) + PVdF (10%), casted on copper foil (photocatalytic reduction)

Table 2. Main features of the cathodic and anodic peaks recorded during the 2nd cycle of the cyclic voltammetry on TiO_2-100, TiO_2-rGO(chem) and TiO_2-rGO(phot) electrodes (rGO loadings 5%). (scan rate = 0.1 mV s^{-1}).

Sample	***TiO_2 -N100***	***TiO_2-rGO(chem)***	***TiO_2-rGO(phot)***
Cathodic Peak			
Potential vs Li^+/Li (V)	1.71	1.72	1.74
Intensity (mA g^{-1})	-496	-264	-645
Charge (C g^{-1})	44	37	43
Anodic Peak			
Potential vs Li^+/Li (V)	2.02	2.05	2.0
Intensity (mA g^{-1})	700	386	667
Charge (C g^{-1})	49	41	44
Delta V	0.31	0.33	0.26

Captions to Figures

Fig. 1. X-ray Diffraction spectra (from bottom to top) of the graphite used for the synthesis of GO, TiO_2 N100, TiO_2-GO, TiO_2-rGO (chem) and TiO_2-rGO (phot). For all the hybrids GO/rGO loading 5%.

Fig. 2. HR-TEM micrographs of a) TiO_2-GO, b) TiO_2-rGO(chem) and c) TiO_2-rGO(phot) composites. Original magnifications: × 80 k.

Fig. 3. Pore volume distribution and specific surface area (inset) for a) TiO_2 N100, TiO_2-rGO(chem) and TiO_2-rGO(phot) with a 5% rGO loading; b) TiO_2-rGO(phot) with different rGO loadings.

Fig. 4. Thermogravimetric analysis in a) air and b) nitrogen of TiO_2 N100, TiO_2-rGO(chem) and TiO_2-rGO(phot) composites (rGO loading 5%).

Fig. 5. Second cycle of the cyclic voltammetry for TiO_2-N100 (black line), TiO_2-rGO(chem) (red line) and TiO_2-rGO(phot) (blue line). The potential was scanned between 1.0 and 3.0 V vs Li^+/Li for 5 times at 0.1 mV s^{-1}.

Fig. 6. Potential vs. Specific Capacity profiles at 1C (a) and 10C (b) (2^{nd} and 100^{th} cycle respectively) extracted from the galvanostatic cycling test for TiO_2-N100 (black line), TiO_2-rGO(chem) (red line) and TiO_2-rGO(phot) (blue line); c) Specific charge capacity at different C-rate (i.e. C, 5C, 10C, 20C, 30C, 40C and C) of TiO_2-rGO and commercial TiO_2 N100 samples. d) Comparison between the cycling performances of samples reduced with Photocatalytic methods: UV-irradiation occurred in aqueous medium or directly on pre-formed electrode (TiO_2-rGO(phot) and TiO_2-rGO(photEL), respectively).

Fig. 7. Specific capacity upon charge/discharge cycles for (a) TiO_2-rGO(chem) (b) and TiO_2-rGO(phot) b), with different amount of GO loading (i.e from 0.5% up to 20%).

Fig. 8. Average specific capacity for each C-rate tested of (a) TiO_2-rGO(chem) and (b) TiO_2-rGO(phot) as a function of the C-rate itself for the samples at 0, 5, 10 and 20% of rGO.

References

[1] R. Schmid, C. Pillot, Introduction to Energy Storage with Market Analysis and Outlook, Review on electrochemical storage materials, 1597 (2014) 3–13.

[2] Every Last Drop: Micro- And Mild Hybrids Drive a Huge Market for Fuel-Efficient Vehicles, Lux Research report, https://portal.luxresearchinc.com/research/report_excerpt/9548

[3] T. Horiba, Lithium-Ion Battery Systems, Proc. IEEE 102 (2014) 939–950.

[4] G. Fabbri, F. Mascioli, F.M. Frattale, M. Pasquali, F. Mura, A. Dell'Era, Automotive Application of Lithium-ion batteries: a new generation of electrode materials, 2013 IEEE International Symposium on Industrial Electronics (ISIE) 2013, doi:10.1109/ISIE.2013.6563857.

[5] S. Goriparti, E. Miele, F. De Angelis, E. Di Fabrizio, R. Proietti Zaccaria, C. Capiglia, Review on recent progress of nanostructured anode materials for Li-ion batteries, J. Pow. Sources 257 (2014) 421–443.

[6] S. Liu, L.Wen, J. Chen, J.-G. Li, X. Sun, X. Li, Sub-20 nm anatase uniformly anchored on graphene oxide and reduced graphene oxide nanosheets and their photocatalytic oxidation and Li-ion storage capabilities, Ceramics International 42 (2016) 3907- 3915.

[7] S. Jiang, R. Wang, M. Pang, H. Wang, S. Zeng, X. Yue, L. Ni, Y. Yu, J. Dai, S. Qiu, Z. Zhang, Assembling porous carbon-coated TiO_2(B)/anatese nanosheets on reduced graphene oxide for high performance lithium-ion batteries, Electrochimica Acta 182 (2015) 406-415.

[8] S. Casino, F. Di Lupo, C. Francia, A. Tuel, S. Bodoardo, C. Gerbaldi, Surfactant-assisted sol gel preparation of high-surface area mesoporous TiO_2 nanocrystalline Li-ion battery anodes, J. Alloys Comp. 594 (2014) 114–121.

[9] T. Fröschl, U. Hörmann, P. Kubiak, G. Kučerová, M. Pfanzelt, C.K. Weiss, R.J. Behm, N. Hüsing, U. Kaiser, K. Landfester, M. Wohlfahrt-Mehrens, High surface area crystalline titanium dioxide: potential and limits in electrochemical energy storage and catalysis, Chem. Soc. Rev. 41 (2012) 5313–5360.

[10] M. Fehse, F. Fischer, C. Tessier, L. Stievano, L. Monconduit, Tailoring of phase composition and morphology of TiO_2-based electrode materials for lithium-ion batteries, J. Power Sources 231 (2013) 23–28.

[11] X. Xin, X. Zhou, J. Wu, X. Yao, Z. Liu, Scalable Synthesis of TiO_2/Graphene Nanostructured Composite with High-Rate Performance for Lithium Ion Batteries, ACS Nano 6 (2012) 11035–11043.

[12] S.H. Nam, H. Shim, Y. Kim, M.A. Dar, J.G. Kim, W.B. Kim, Z. Yang, Ag or Au Nanoparticle-Embedded One-Dimensional Composite TiO_2 Nanofibers prepared via Electrospinning for Use in Lithium-Ion Batteries, ACS Appl. Mater. Interfaces 2 (2010) 2046–2052.

[13] K. Shyamal, S.K. Das, M. Patel, J.A. Bhattacharyya, Effect of Nanostructuring and Ex situ Amorphous Carbon Coverage on the Lithium Storage and Insertion Kinetics in Anatase Titania, ACS Appl. Mater. Interfaces 2 (2010) 2091–2099.

[14] H. Geng, X. Cao, Y. Zhang, K. Geng, G. Qu, M. Tang, J. Zheng, Y. Yang, H. Gu, Hollow nanospheres composed of titanium dioxide nanocrystals modified with carbon and gold for high performance lithium ion batteries, J. Pow. Sources 294 (2015) 465-472.

[15] J. Qiu, C. Lai, Y. Wang, S. Li, S. Zhang, Resilient mesoporous TiO_2/graphene nanocomposite for high rate performance lithium-ion batteries, Chem. Eng. J. 256 (2014) 247–254.

[16] W. Li, F. Wang, S. Feng, J. Wang, Z. Sun, B. Li, Y. Li, J. Yang, A.A. Elzatahry, Y. Xia, D. Zhao, Sol–Gel Design Strategy for Ultradispersed TiO_2 Nanoparticles on Graphene for High-Performance Lithium Ion Batteries, J. Am. Chem. Soc. 135 (2013) 18300–18303.

[17] Y. Xie, J. Song, P. Zhou, Y. Ling, Y. Wu, Controllable synthesis of TiO_2/graphene nanocomposites for long lifetime lithium storage: nanoparticles vs. nanolayers, Electrochimica Acta 210 (2016) 358-366.

[18] Y. Ren, J. Zhang, Y. Liu, H. Li, H. Wei, B. Li, X. Wang, Synthesis and Superior Anode Performances of TiO_2-Carbon-rGO Composites in Lithium-Ion Batteries, ACS Appl. Mater. Interfaces 4 (2012) 4776–4780.

[19] M. Zhen, X. Guo, G. Gao, Z. Zhou, L. Liu, Rutile TiO_2 nanobundles on reduced graphene oxides as anode materials for Li ion batteries, Chem. Commun. 50 (2014) 11915–11918.

[20] X. Sun, Y. Zhang, Lin Gu, Lilei Hu, Kun Feng, Zhongwei Chen, Bo Cui, Nanocomposite of TiO_2 Nanoparticles-Reduced Graphene Oxide with High-Rate Performance for Li-Ion Battery, ECS Trans. 64 (2015) 11–17.

[21] F. Li, J. Jiang, X. Wang, F. Liu, J. Wang, Y. Chen, S. Han, H. Lin, Assembly of TiO_2/graphene with macroporous 3D network framework as an advanced anode material for Li-ion batteries, RCS Adv 6 (2016) 3335-3340.

[22] J. Qiu, P. Zhang, M. Ling, S. Li, P. Liu, H. Zhao, S. Zhang, Photocatalytic Synthesis of TiO_2 and Reduced Graphene Oxide Nanocomposite for Lithium Ion Battery, ACS Appl. Mater. Interfaces 4 (2014) 3636–3642.

[23] D. Wang, D. Choi, J. Li, Z. Yang, Z. Nie, R. Kou, D. Hu, C. Wang, L.V. Saraf, J. Zhang, I.A. Aksay, J. Liu, Self-Assembled TiO_2–Graphene Hybrid Nanostructures for Enhanced Li-Ion Insertion, ACS Nano 3 (2009) 907–914.
[24] E. Sheha, Studies on TiO_2/Reduced Graphene Oxide Composites as Cathode Materials for Magnesium-Ion Battery, Graphene 3 (2014) 36–43.
[25] P. Muthirulan, C. Nirmala Devi, M. Meenakshi Sundaram, A green approach to the fabrication of titania–graphene nanocomposites: Insights relevant to efficient photodegradation of Acid Orange 7 dye under solar irradiation, Mater. Sci. Semicond. Process. 25 (2014) 219–230.
[26] Z. Yao, M. Wang, S. Sun, R. Jia, H. Li, High Performance Photocatalysts Based on N-doped Graphene-P25 for Photocatalytic Reduction of Carbon Tetrachloride, J. Inorg. Organomet. Polym. 24 (2014) 315–320.
[27] L. Staudenmaier, Method of preparation of graphite-acid, Berichte der Deutschen Chemishen Gesellschaft 31 (1898) 1481–1499.
[28] W.S. Hummers, R.E. Offeman, Preparation of graphitic oxide, J. Am. Chem. Soc. 80 (1958) 1339.
[29] N.M. Huang, H.N. Lim, C.H. Chia, M.A. Yarmo, M.R. Muhamad, Simple room-temperature preparation of high-yield large-area graphene oxide, Int. J. Nanomed. 6 (2011) 3443–3448.
[30] M. Minella, M. Demontis, M. Sarro, F. Sordello, P. Calza, C. Minero, Photochemical stability and reactivity of Graphene Oxide, J. Mater Sci. 50 (2015) 2399–2409.
[31] M. Bruna, B. Massessi, C. Cassiago, A. Battiato, E. Vittone, G. Speranza, S. Borini, Synthesis and properties of monolayer graphene oxyfluoride, J. Mater. Chem. 51 (2011) 18730–18737.
[32] J. Shang, L. Ma, J. Li, W. Ai, T. Yu, G.G. Gurzadyan, The Origin of Fluorescence from Graphene Oxide, Sci. Rep. 2 (2012) 792, DOI: 10.1038/srep00792.
[33] L. Dong, M. Li, L. Dong, M. Zhao, J. Feng, Y. Han, J. Deng, X. Li, D. Li, X. Sun, Hydrothermal synthesis of mixed crystal phases TiO_2–reduced graphene oxide nanocomposites with small particle size for lithium ion batteries, J. Hydrogen Energy 38 (2014) 1–7.
[34] H. Cao, B. Li, J. Zhang, F. Lian, X. Kong, M. Qu, Synthesis and superior anode performance of TiO_2@reduced graphene oxide nanocomposites for lithium ion batteries, J. Mater. Chem. 22 (2012) 9759–9766.
[35] S.K. Das, A.J. Bhattacharyya, Influence of Mesoporosity and Carbon Electronic Wiring on Electrochemical Performance of Anatase Titania, J. Electrochem. Soc. 158 (2011) A705–A710.
[36] S. Ding, J.S. Chen, D. Luan, F.Y. Chiang Boey, S. Madhavi, X. Wen Lou, Graphene-supported anatase TiO_2 nanosheets for fast lithium storage, Chem. Commun. 47 (2011) 5780–5782.

[37] B.Y.S. Chang, N.M. Huang, M.N. An'amt, A.R. Marlinda, Y. Norazriena, M.R. Muhamad, I. Harrison, H.N. Lim, C.H. Chia, Facile hydrothermal preparation of titanium dioxide decorated reduced graphene oxide nanocomposites, Int. J. Nanomed. 7 (2012) 3379–3387.

[38] Q. Zhang, Y.Q. He, X.G. Chen, D.H. Hu, L.J. Li, T. Yin, L.L. Ji, Structure and photocatalytic properties of TiO_2-Graphene Oxide intercalated composite, Chinese Sci. Bulletin 56 (2011) 331–339.

[39] H.C. Schniepp, J.L. Li, M.J. McAllister, H. Sai, M. Herrera-Alonso, D.H. Adamson, Functionalized Single Graphene Sheets Derived from Splitting Graphite Oxide, J. Phys. Chem. B 110 (2006) 8535–8539.

[40] L.J. Cote, R. Cruz-Silva, J. Huang, Flash Reduction and Patterning of Graphite Oxide and Its Polymer Composite, J. Am. Chem. Soc. 131 (2009) 11027–11032.

[41] D.A.H. Hanaor, C.C. Sorrell, Review of the anatase to rutile phase transformation, J. Mater. Sci. 46 (2011) 855–874.

[42] F. Di Lupo, A. Tuel, V. Mendez, C. Francia, G. Meligrana, S. Bodoardo, C. Gerbaldi, Mesoporous TiO_2 nanocrystals produced by a fast hydrolytic process as high-rate long-lasting Li-ion battery anodes, Acta Materialia 69 (2014) 60–67.

[43] Z. Yang, D. Choi, S. Kerisit, K.M. Rosso, D. Wang, J. Zhang, G. Graff, J. Liu, Nanostructures and lithium electrochemical reactivity of lithium titanites and titanium oxides: A review, J. Power Sources 192 (2009) 588–598.

[44] V. Subramanian, A. Karki, K.I. Gnanasekar, Fannie Posey Eddy, B. Rambabu, Nanocrystalline TiO_2 (anatase) for Li-ion batteries, J. Power Sources 159 (2006) 186–192.

[45] S. Pei, H.-M. Cheng, The reduction of graphene oxide, Carbon 50 (2012) 3210–3228.

Fig. 1

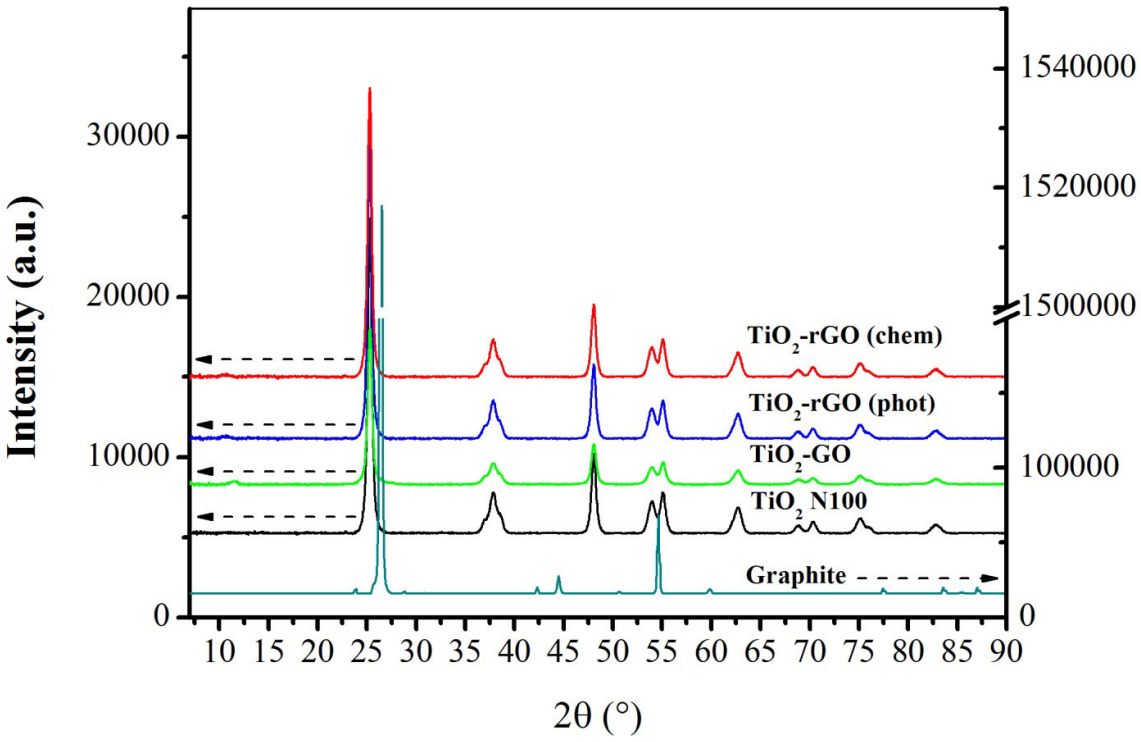
Intensity (a.u.)
30000
20000
10000
0
1540000
1520000
1500000
100000
0
TiO2-rGO (chem)
TiO2-rGO (phot)
TiO2-GO
TiO2 N100
Graphite
10 15 20 25 30 35 40 45 50 55 60 65 70 75 80 85 90
2θ (°)

Fig.2

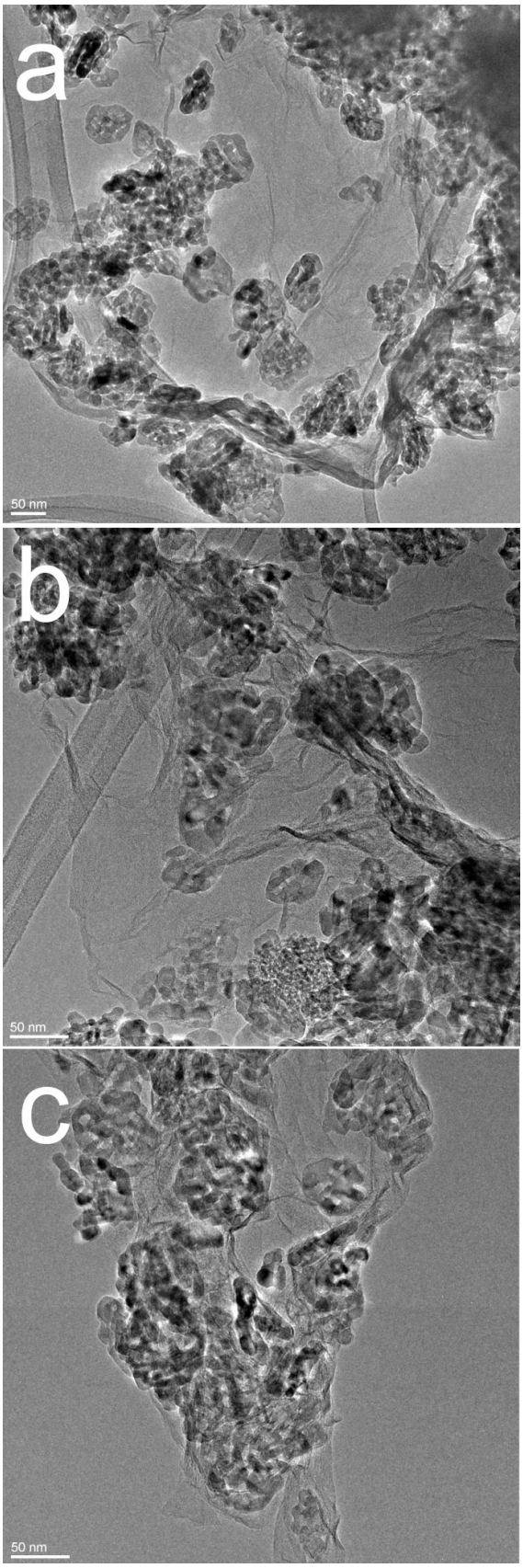

Fig.3

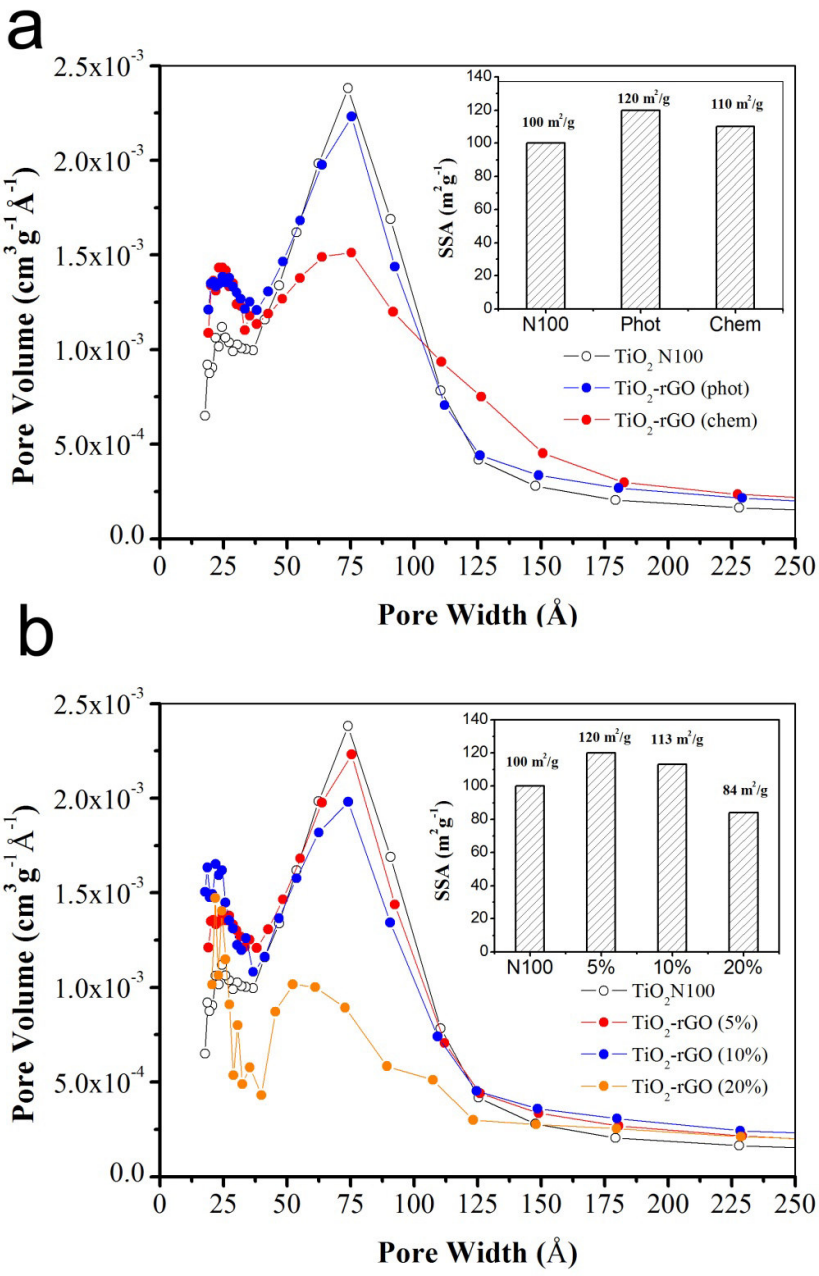
a
Pore Volume (cm^3 g^{-1} Å^{-1})
Pore Width (Å)
SSA (m^2 g^{-1})
100 m^2/g
120 m^2/g
110 m^2/g
N100
Phot
Chem
TiO$_2$ N100
TiO$_2$-rGO (phot)
TiO$_2$-rGO (chem)
b
Pore Volume (cm^3 g^{-1} Å^{-1})
Pore Width (Å)
SSA (m^2 g^{-1})
100 m^2/g
120 m^2/g
113 m^2/g
84 m^2/g
N100
5%
10%
20%
TiO$_2$N100
TiO$_2$-rGO (5%)
TiO$_2$-rGO (10%)
TiO$_2$-rGO (20%)

Fig.4

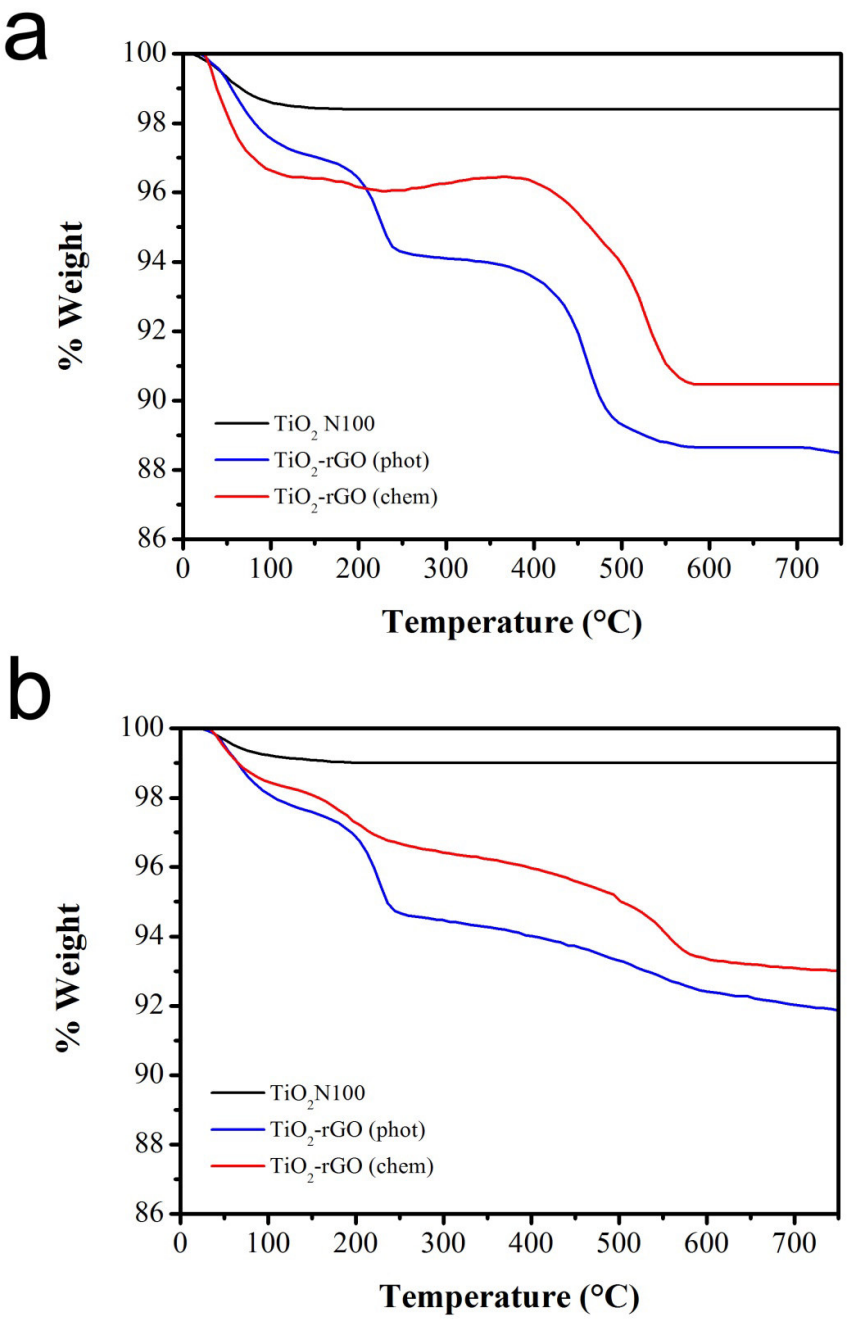
a
100
98
96
94
92
90
88
86
% Weight
TiO2 N100
TiO2-rGO (phot)
TiO2-rGO (chem)
0
100
200
300
400
500
600
700
Temperature (°C)
b
100
98
96
94
92
90
88
86
% Weight
TiO2N100
TiO2-rGO (phot)
TiO2-rGO (chem)
0
100
200
300
400
500
600
700
Temperature (°C)

Fig.5

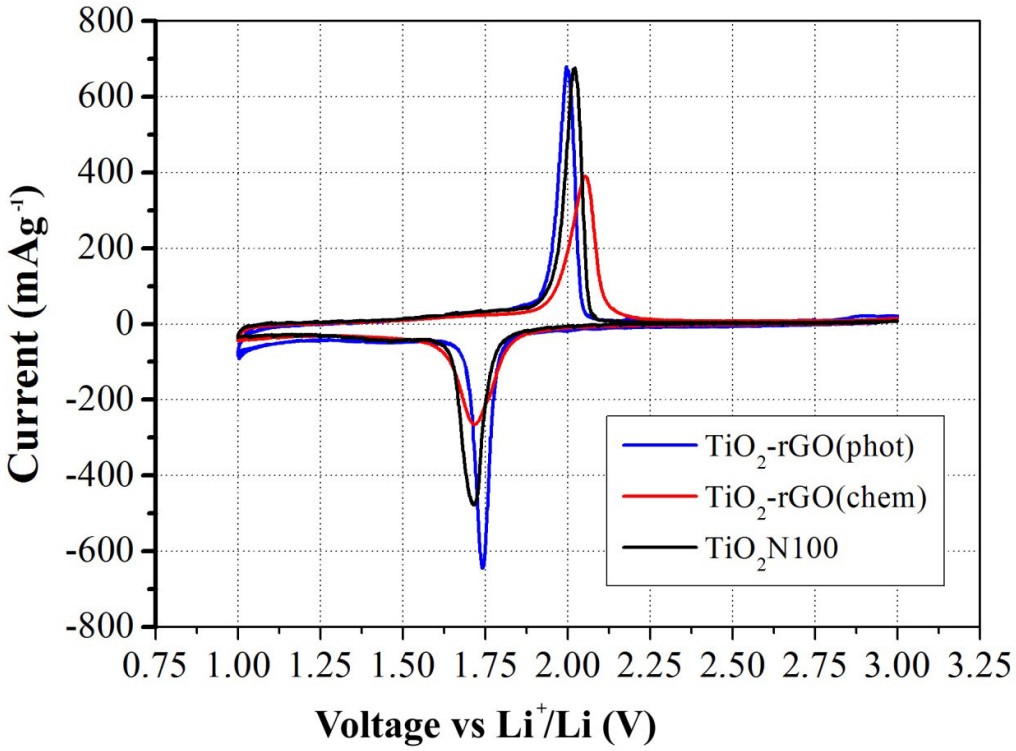
800
600
400
200
0
-200
-400
-600
-800
Current (mAg-1)
0.75 1.00 1.25 1.50 1.75 2.00 2.25 2.50 2.75 3.00 3.25
Voltage vs Li+/Li (V)
TiO2-rGO(phot)
TiO2-rGO(chem)
TiO2N100

Fig.6

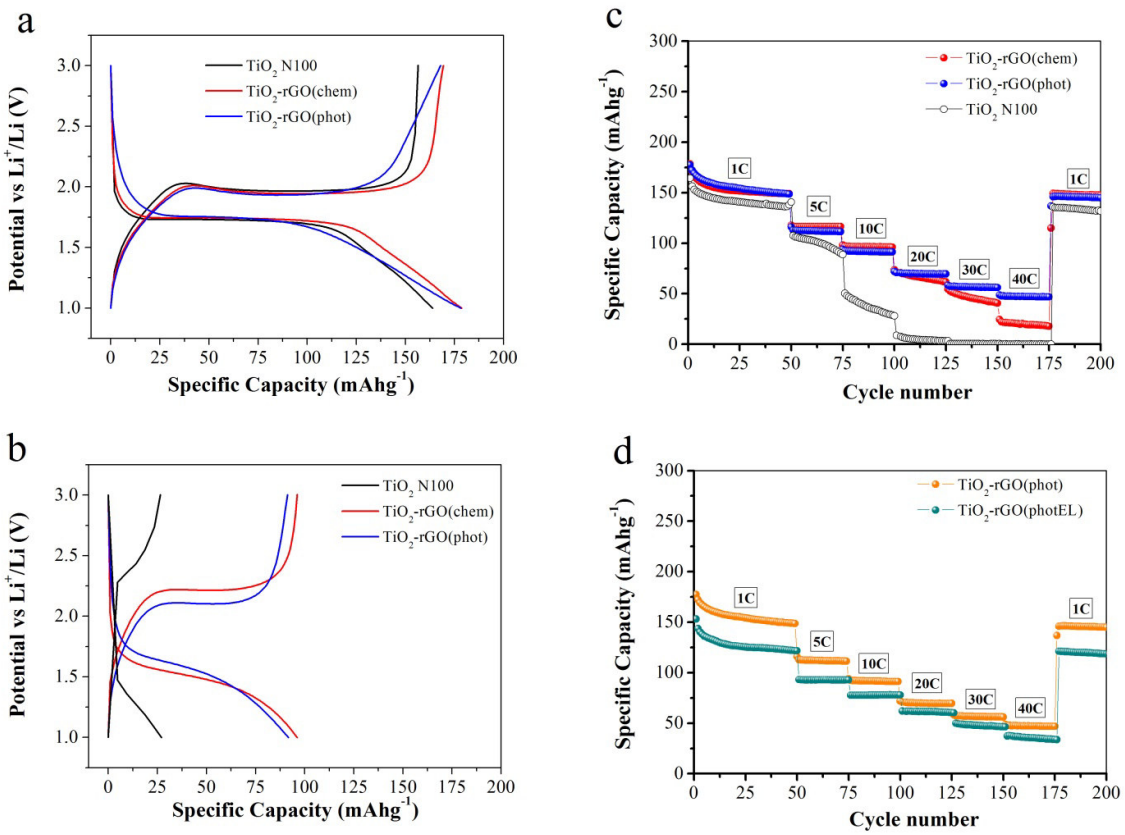
a
Potential vs Li+/Li (V)
Specific Capacity (mAhg-1)
TiO2 N100
TiO2-rGO(chem)
TiO2-rGO(phot)
b
Potential vs Li+/Li (V)
Specific Capacity (mAhg-1)
TiO2 N100
TiO2-rGO(chem)
TiO2-rGO(phot)
c
Specific Capacity (mAhg-1)
Cycle number
TiO2-rGO(chem)
TiO2-rGO(phot)
TiO2 N100
1C
5C
10C
20C
30C
40C
1C
d
Specific Capacity (mAhg-1)
Cycle number
TiO2-rGO(phot)
TiO2-rGO(photEL)
1C
5C
10C
20C
30C
40C
1C

Fig.7

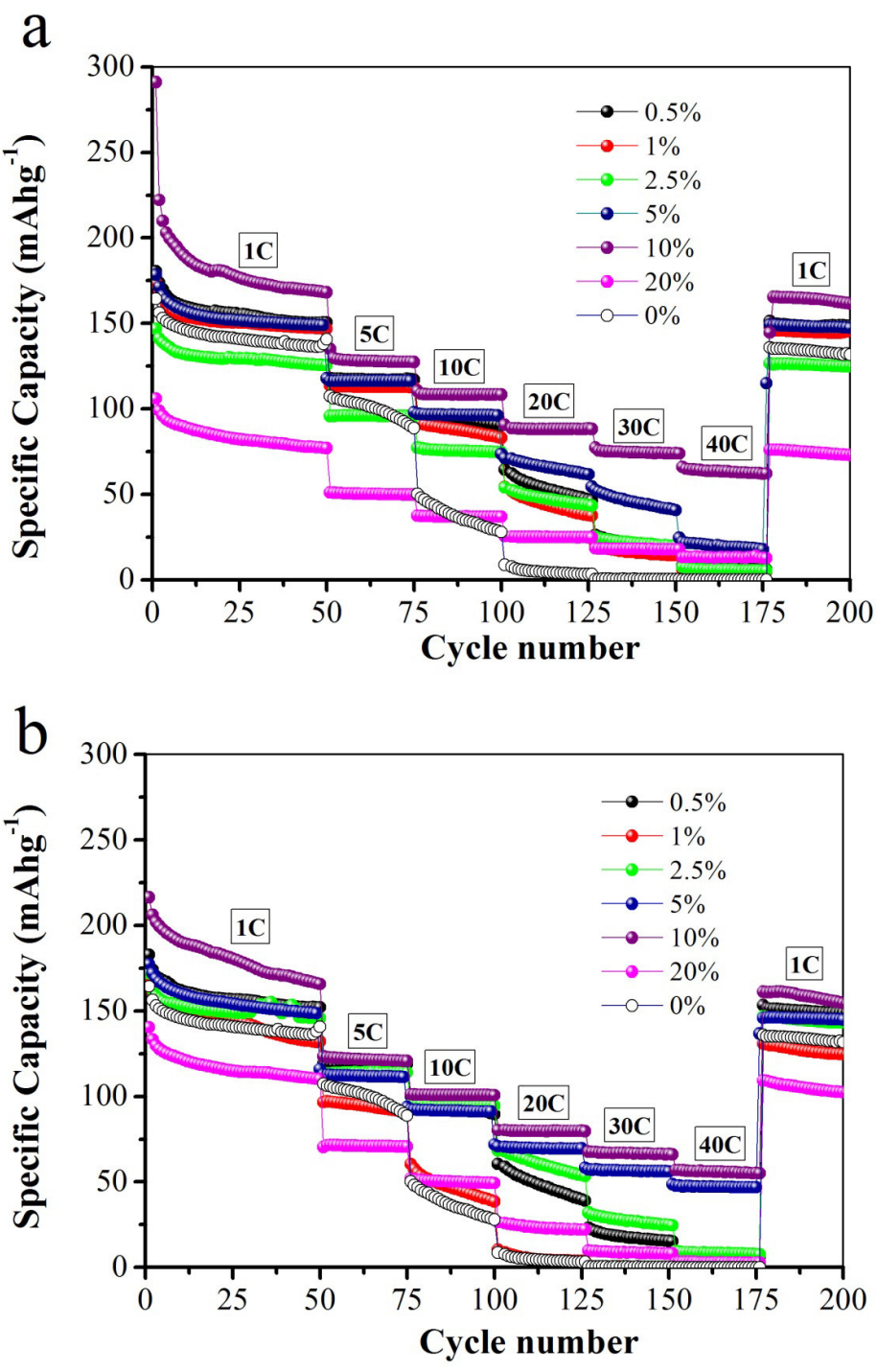
a
b
Specific Capacity (mAhg-1)
Cycle number
0.5%
1%
2.5%
5%
10%
20%
0%
1C
5C
10C
20C
30C
40C
1C
0
25
50
75
100
125
150
175
200
0
50
100
150
200
250
300

Fig.8

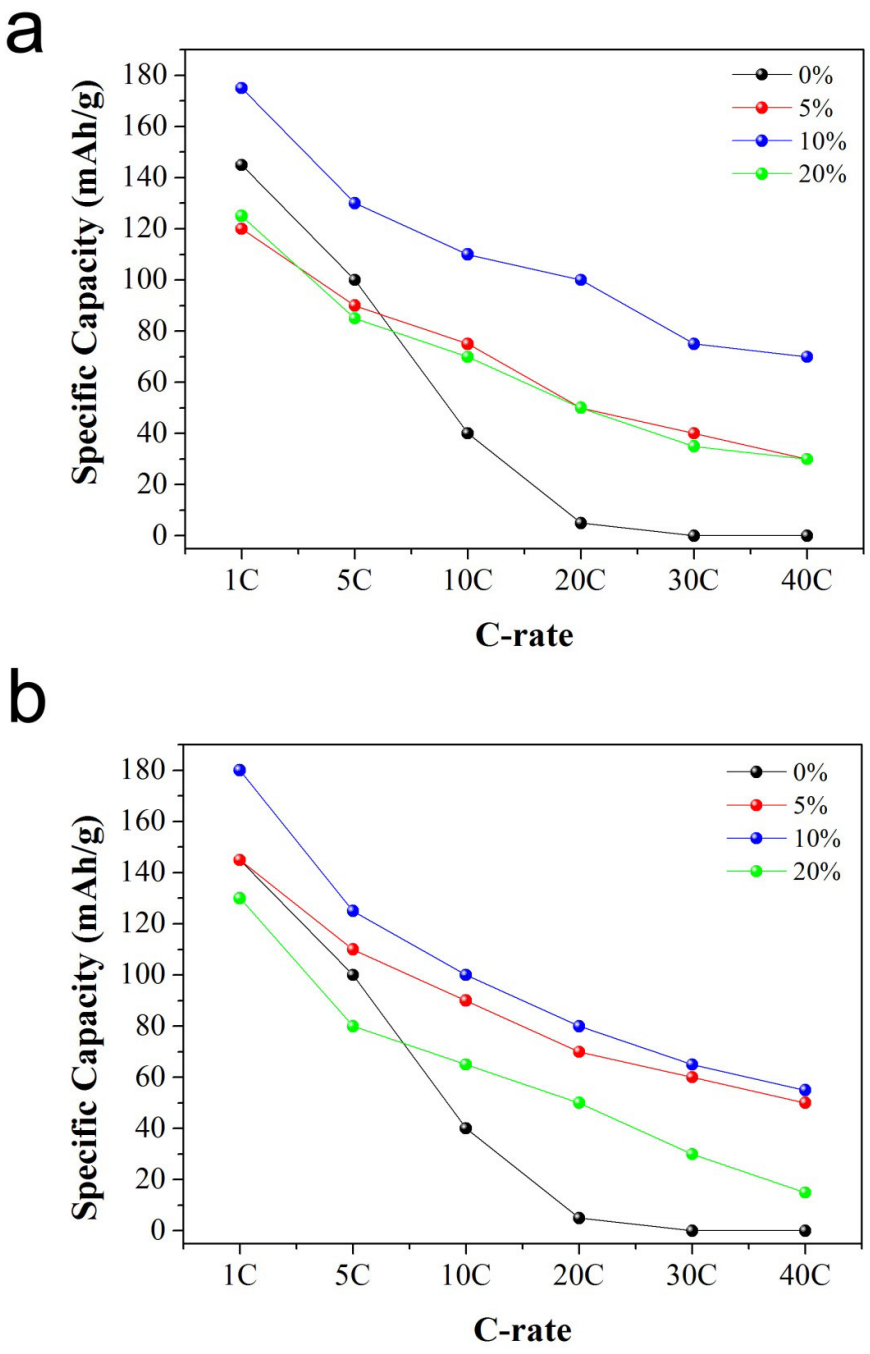
a
Specific Capacity (mAh/g)
0
20
40
60
80
100
120
140
160
180
1C
5C
10C
20C
30C
40C
C-rate
0%
5%
10%
20%
b
Specific Capacity (mAh/g)
0
20
40
60
80
100
120
140
160
180
1C
5C
10C
20C
30C
40C
C-rate
0%
5%
10%
20%

Supplementary Data

Anodic Materials for Lithium-ion Batteries: TiO_2-rGO Composites for High Power Applications

*Marco Minella[a], Daniele Versaci[b], Simone Casino[b], Francesca Di Lupo[b], Claudio Minero[a], Alfio Battiato[c], N. Penazzi[b], Silvia Bodoardo[b]**

[a] Department of Chemistry and NIS Centre of Excellence, University of Torino, via P. Giuria 5, Torino,10125, Italy

[b] Gruppo di Elettrochimica - Department of Applied Science and Technology, Politecnico di Torino, c.so Duca degli Abruzzi 24, 10129 Torino, Italy

[c] Department of Experimental Physics and NIS Centre of Excellence, University of Torino, via P. Giuria 1, Torino, 10125, Italy

ESCA-XPS characterization of the TiO_2-rGO samples

The full range XPS spectra of the studied materials are reported in Fig. S1 of the Supplementary Data. In all the cases the spectra are dominated by the peaks of titanium (Ti2p doublet), oxygen (O Auger series and O1s core line) and carbon (C1s), thus confirming the absence of foreign elements in the structure of the produced materials. More detailed information was obtained from the analysis of each single photoelectric core line, which were acquired using a higher resolution and longer acquisition time respect to the survey spectra. The binding energy (BE) and the % atomic relative concentration of each deconvoluted component were summarized in the tables reported in SI (from Table S1 to Table S6).

In all the samples the main peak of titanium is located around 459 eV, energy value in good agreement with the ones reported for TiO_2 crystalline structure [1]. The principal line of the oxygen can be splitted into a main component at 530 eV related to the oxygen in the TiO_2 structure and one or two components at higher BE (532-533 eV) due to the presence of C-O and C-OH bonds in the GO and rGO phases [2]. Note that the relative atomic abundance of titanium and oxygen in the sample is in all the cases equal to 1:2, as predicted by the stoichiometry and as a consequence of the absence of significant modifications of the TiO_2 structure with the adopted treatments. The experimental uncertainty related to the evaluation of the atomic relative concentration is in the 3-4% range.

From the deconvolution of the C1s signals it was possible to infer about the modifications of the oxidation state of carbon before and after the different reduction procedure. Fig. S2 shows the overlap of the C1s signals (normalized) for the investigated samples. The spectrum of TiO_2-GO is dominated by two main overlapped peaks while in the case of reduced samples only a main peak dominates the spectra with a complex shoulder at higher BE.

[1] A.V. Naumkin, A. Kraut-Vass, S.W. Gaarenstroom, C.J. Powell, NIST X-ray Photoelectron Spectroscopy Database. NIST Standard Reference Database 20, Version 4.1, http://srdata.nist.gov/xps/selEnergyType.aspx, last access 19th July 2016

[2] L.J. Cote, R. Cruz-Silva, J. Huang, Flash Reduction and Patterning of Graphite Oxide and Its Polymer Composite, J. Am. Chem. Soc. 131 (2009) 11027–11032.

Fig. S3 shows the deconvolution of the C1s peak in its main Gaussian components. The fitting of the C1s peak of TiO_2-GO hybrid (Fig. S3a) shows the presence of three peaks centered at 284.6, 286.6 and 288.9 eV, respectively. The peak at lower BE is related to carbon in sp^2 hybridization condition typical of graphitic/graphenic structures. While the components at higher BE can be related to carbon atom in higher state of oxidation. The relative weight of the graphenic carbon with respect to the oxidized one is roughly equal to 43.8 % (see Table S2). The results of the reduction procedure are well seen in Fig. S3b and S3c. The spectra of the TiO_2-rGO(chem.) and TiO_2-rGO(phot) are quite similar. In both cases the main component is the peak due to the graphenic carbon, while the related shoulder can be fitted with at least four other components. Interesting, in both cases the relative weight of the graphenic carbon with respect to the oxidized one increase to 57.3 % and 51.5 % for the TiO_2-rGO(chem.) and TiO_2-rGO(phot), respectively, as a proof of an effective reduction of the GO structure (see Table S4 and S6). Note that the higher degree of reduction has been obtained by the chemical reduction.

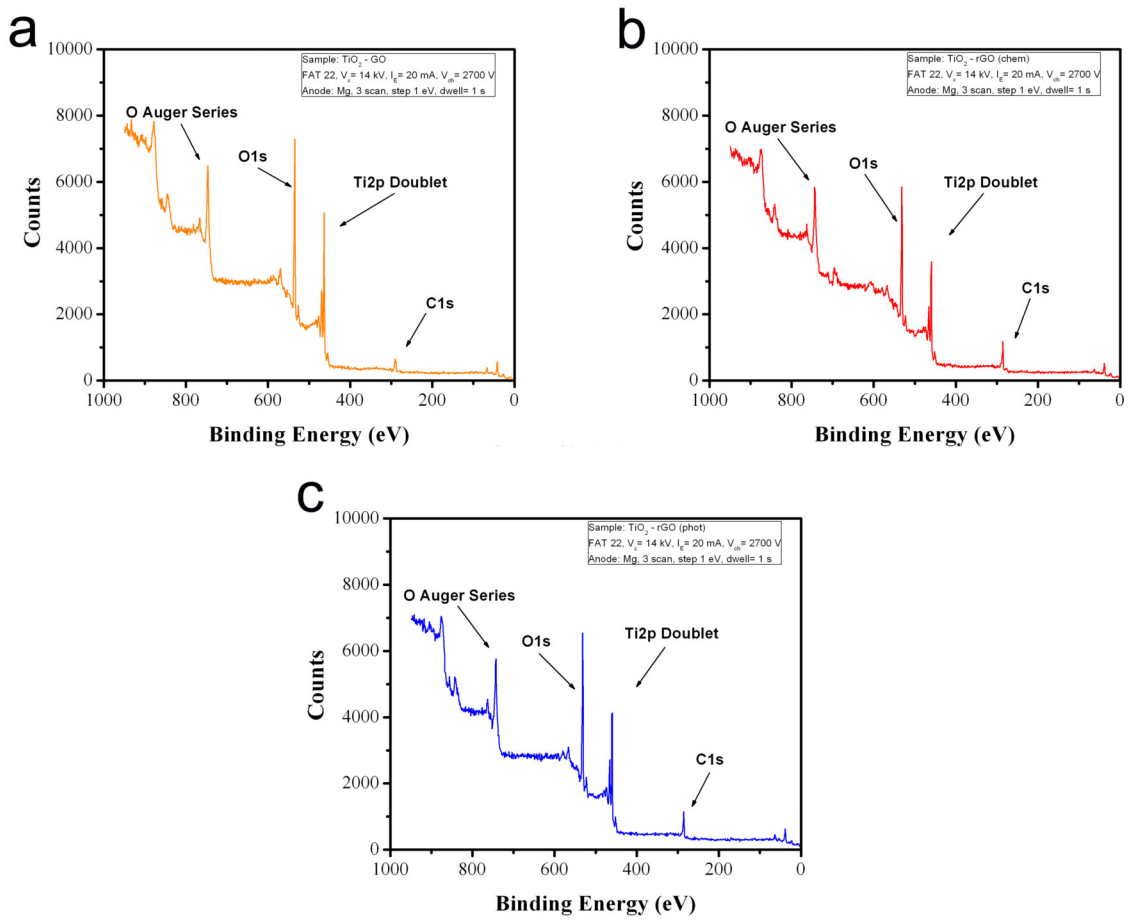

Fig. S1 Survey XPS spectrum of a) TiO_2- GO, b) TiO_2-rGO(chem), c) TiO_2-rGO(phot).

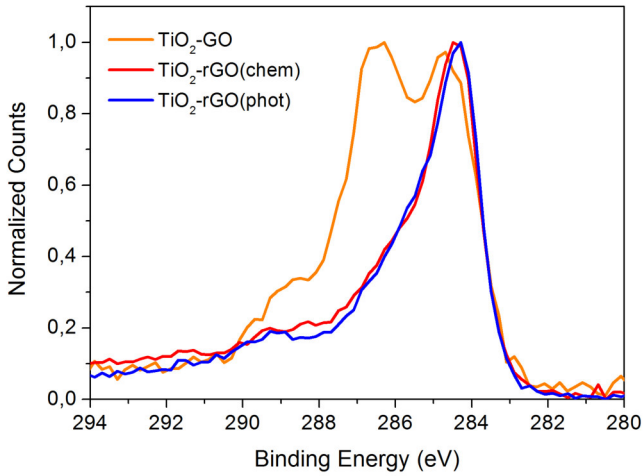

Fig. S2. XPS of C1s core lines for TiO_2-rGO and TiO_2-GO composites (GO/rGO loading 5%).

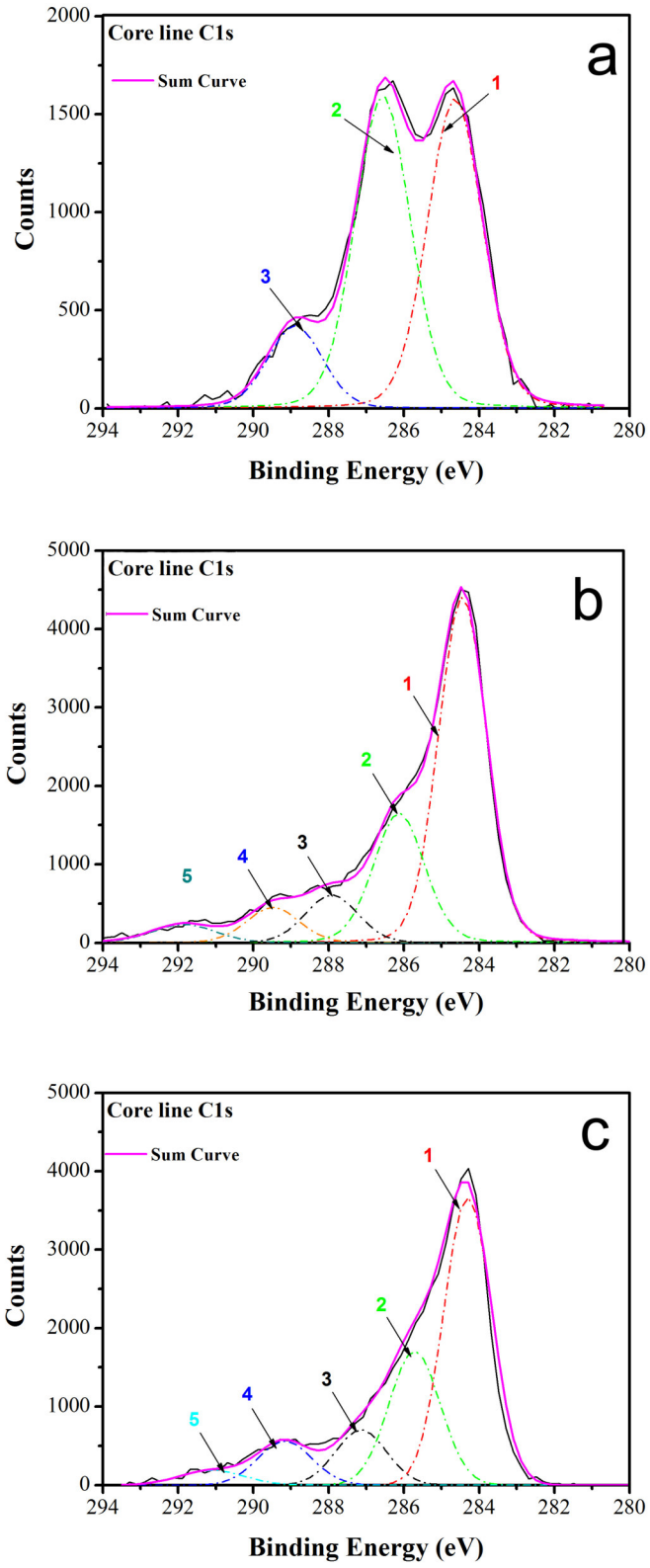

Fig. S3. Peak deconvolution of C(1s) XPS core level of a) TiO2- GO, b) TiO2-rGO(chem) and c) TiO2-rGO(phot) with a 5% GO/rGO loading.

Table S1. Description of bonds and atomic abundances calculated from the fitted components of C, O and Ti core peaks for TiO_2 – GO (GO loading 5%).

Component	*BE (eV)*	*Conc. at %*	*Atomic content*
C1s	284.6	8.5	19.4
C1s	286.6	8.6	
C1s	288.9	2.3	
O1s	530.3	43.7	59.8
O1s	532.0	12.2	
O1s	533.0	4.0	
Ti2p	459.2	20.8	20.8

Table S2. XPS data of TiO_2–GO deconvoluted into three peaks; Binding energies (eV) and relative area percentages for C1s.

Component	*BE (eV)*	*Conc. at %*	*Atomic content*
C1s	284.6	43.8	100
C1s	286.6	44.6	
C1s	288.9	11.7	

Table S3. Description of bonds and atomic abundances calculated from the fitted components of C, O and Ti core peaks for TiO_2 – rGO(chem) (rGO loading 5%).

Component	*BE (eV)*	*Conc. at %*	*Atomic content*
C1s	284.4	20.1	35.1
C1s	286.1	8.2	
C1s	289.5	2.3	
C1s	291.9	1.4	
C1s	287.9	3.1	
O1s	530.5	37.2	49.1
O1s	532.2	9.4	
O1s	533.72	2.42	
Ti2p	459.15	15.88	15.88

Table S4. XPS data of TiO_2 – rGO(chem) deconvoluted into five peaks; Binding energies (eV) and relative area percentages for C1s.

Component	*BE (eV)*	*Conc. at %*	*Atomic content*
C1s	284.4	57.3	100
C1s	286.1	23.3	
C1s	289.5	6.6	
C1s	291.9	4.1	
C1s	287.9	8.7	

Table S5. Description of bonds and atomic abundances calculated from the fitted components of C, O and Ti core peaks for TiO_2–rGO(phot) (rGO loading 5%).

Component	*BE (eV)*	*Conc. at %*	*Atomic content*
C1s	284.3	15.9	30.9
C1s	285.7	7.9	
C1s	287.1	3.3	
C1s	289.2	2.8	
C1s	291.1	1.1	
O1s	530.8	40.8	49.9
O1s	532.8	9.1	
Ti2p	459.4	19.2	19.2

Table S6. XPS data of TiO_2 – rGO(phot) deconvoluted into five peaks; Binding energies (eV) and relative area percentages for C1s.

Component	*BE (eV)*	*Conc. at %*	*Atomic content*
C1s	284.3	51.5	100.0
C1s	285.7	25.6	
C1s	287.1	10.5	
C1s	289.2	8.9	
C1s	291.1	3.5	